Shadowed Fading in Indoor Off-Body Communication Channels: A Statistical Characterization Using the $\kappa-\mu$/Gamma Composite Fading Model

Seong Ki Yoo, *Student Member, IEEE*, Simon L. Cotton, *Senior Member, IEEE*, Paschalis C. Sofotasios, *Member, IEEE*, and Steven Freear, *Senior Member, IEEE*

Abstract—This paper investigates the characteristics of the shadowed fading observed in off-body communications channels at 5.8 GHz. This is realized with the aid of the $\kappa-\mu$/gamma composite fading model, which assumes that the transmitted signal undergoes $\kappa-\mu$ fading, which is subject to multiplicative shadowing. Based on this, the total power of the multipath components, including both the dominant and scattered components, is subject to non-negligible variations that follow the gamma distribution. For this model, we present an integral form of the probability density function (PDF) as well as important analytic expressions for the PDF, cumulative distribution function, moments, and moment generating function. In the case of indoor off-body communications, the corresponding measurements were carried out in the context of four explicit individual scenarios, namely: line of sight (LOS), non-LOS walking, rotational, and random movements. The measurements were repeated within three different indoor environments and considered three different hypothetical body worn node locations. With the aid of these results, the parameters for the $\kappa-\mu$/gamma composite fading model were estimated and analyzed extensively. Interestingly, for the majority of the indoor environments and movement scenarios, the parameter estimates suggested that dominant signal components existed even when the direct signal path was obscured by the test subject's body. In addition, it is shown that the $\kappa-\mu$/gamma composite fading model provides an adequate fit to the fading effects involved in off-body communications channels. Using the Kullback–Leibler divergence, we have also compared our results with another recently proposed shadowed fading model, namely, the $\kappa-\mu$/lognormal LOS shadowed fading model. It was found that the $\kappa-\mu$/gamma composite fading model provided a better fit for the majority of the scenarios considered in this paper.

Index Terms—Body shadowing, channel characterization, off-body communications, path loss, shadowed fading models.

I. INTRODUCTION

IN BODY centric communications, while path loss, large-scale and small-scale fading phenomena can be responsible for shaping the characteristics of the received signal, they are often superseded by body shadowing as the predominant fading mechanism. In off-body communications, one or more wireless devices are positioned on the human body and communicate with a local transceiver or a base station in a different physical location. In this case, the shadowing effects typically occur due to the obstruction of the direct signal path by the user's body and/or surrounding people and obstacles [1]–[3]. As a consequence, the received signal can experience deep fades which reduce the overall signal reliability and ultimately the information recovering capability. Indicatively, it was observed in [3] that deep fades of up to 67 dB, directly attributable to the body shadowing, were possible when a person rotated within the immediate vicinity of a hypothetical base station antenna.

The characteristics of off-body communications channels have been previously studied for different operating frequencies, types of antenna, multipath environments, user movements, and body worn node locations [3]–[9]. These studies have shown that the shadowing of the received signal was sensitive not only to the user movement but also to the position of the wireless node on the body. For example in [5], a number of off-body communications channels operating at 2.45 GHz within a multipath environment were investigated. Four possible body worn node locations (head, left arm, right arm and back) and two user movements (walking and running) were considered. It was found that radio channel parameters such as the received signal power, delay spread and direction of arrival were strongly dependent upon the antenna placement and the user movement. For instance, while the test subject was running, a left-arm positioned antenna spent more time

S. K. Yoo and S. L. Cotton are with the Institute of Electronics, Communications and Information Technology, Queen's University Belfast, Belfast BT3 9DT, U.K. (e-mail: syoo02@qub.ac.uk; simon.cotton@qub.ac.uk).

P. C. Sofotasios was with the Department of Electronic and Electrical Engineering, University of Leeds, Leeds LS2 9JT, U.K. He is now with the Department of Electronics and Communications Engineering, Tampere University of Technology, Tampere 33101, Finland, and also with the Department of Electrical and Computer Engineering, Aristotle University of Thessaloniki, Thessaloniki 54124, Greece (e-mail: p.sofotasios@ieee.org).

S. Freear is with the Department of Electronic and Electrical Engineering, University of Leeds, Leeds LS2 9JT, U.K. (e-mail: s.freear@leeds.ac.uk).

under the line of sight (LOS) conditions than in the case of the walking scenario.

In the same context, it was observed in [7] that the corresponding mean channel gain strongly depended not only on the body worn node locations but also on the type of antenna employed. In this study, the authors modeled the channel using a combination of the mean channel gain which was characterized through a linear log-distance fit of the data, the small-scale fading component which was modeled by the Nakagami-*m* distribution and the body shadowing effect which was considered as an additional loss contribution to the mean channel gain and hence was described as a function of the body orientation angle. In fact, this decomposition of the received signal into its shadowed and small-scale fading components is common amongst all the analyses presented in [3] and [6]–[9]. However, although this step may simplify the analysis of the channel data, in some respects it seems an unnatural approach as in reality both shadowed and small-scale fading co-exist and consequently affect body centric communications channels simultaneously. Another benefit of using composite fading models to characterize wireless channels is that they circumvent the requirement to choose an appropriate smoothing window size for the computation of the local mean signal. This choice can ultimately impact the parameter estimation process and also any inferences made from the channel data. Therefore, in this paper and based on the aforementioned investigations, we consider a *composite* fading model, which is capable of encapsulating both shadowing and small-scale fading effects as they occur concurrently.

Over the last few decades, various composite fading models have been proposed which combine shadowed and small-scale fading. These can be further divided into *line of sight* and *multiplicative* shadowed fading models. The former relates to random variation of the amplitude of the dominant signal component *only*, which is caused by complete or partial obstruction of the direct signal path. This includes the Rice/lognormal [10], $\kappa-\mu$/lognormal [11], Rice/Nakagami-*m* [12] and $\kappa-\mu$/Nakagami-*m* [13], [14] LOS shadowed fading models. On the contrary, the latter causes random fluctuations of the total power of the multipath components, i.e. *both* the dominant and scattered signal components. This includes Rayleigh/lognormal [15], [16], Rice/lognormal [17], Rayleigh/gamma [18], also known as the *K*-distribution, and Nakagami-*m*/gamma [19], also known as the generalized *K*-distribution, K_G, composite fading models.

The characterization of body centric communications channels using composite fading models has received little attention in the literature. One of the few known studies is reported in [11] where the author characterized the LOS shadowed fading observed in body centric communications channels using the $\kappa-\mu$/lognormal LOS shadowed fading model. While the underlying assumption employed in [11] may hold in some cases, it is also reasonable to assume that in body centric communications, both the dominant and scattered signal components can be shadowed together. Therefore, in this paper, we perform a more general statistical characterization of the shadowed fading for indoor off-body communications channels using

the $\kappa-\mu$/gamma composite fading model, which was initially proposed in [20].

The remainder of this paper is organized as follows: Section II introduces the $\kappa-\mu$/gamma composite fading model. Novel analytic expressions are derived for the fundamental statistical measures of the proposed model while its versatility is also illustrated by highlighting a number of other distributions which are included as special cases. In Section III, the measurement system, environments and scenarios are demonstrated in detail while Section IV presents the off-body channel characterization for each of the considered environments in terms of a path loss model and the shadowed fading parameter estimates alongside some examples of the model fitting. In Section V, the goodness-of-fit of the $\kappa-\mu$/gamma composite fading model is also evaluated and compared with the $\kappa-\mu$/lognormal LOS shadowed fading model both theoretically and experimentally. Finally, Section VI concludes the paper with some closing remarks.

II. THE $\kappa-\mu$/GAMMA COMPOSITE SHADOWED FADING MODEL

A. Formulation of the $\kappa-\mu$/Gamma Distribution

The probability density function (PDF) of the composite signal envelope, R, in a $\kappa-\mu$/gamma shadowed fading channel [20] can be expressed as the integral of the conditional probability density of the $\kappa-\mu$ fading with respect to the random variation of the mean signal power, Ω, as follows

$$f_R(r) = \int_0^\infty f_{R|\Omega}(r \mid \omega) f_\Omega(\omega) \, d\omega \qquad (1)$$

To this effect, if we initially hold the mean signal power constant, then the PDF of the $\kappa-\mu$/gamma composite fading channel in (1) can be expressed as

$$f_{R|\Omega}(r|\omega) = \frac{2\mu(\kappa+1)^{\frac{\mu+1}{2}} r^\mu}{\kappa^{\frac{\mu-1}{2}} \exp(\mu\kappa) \omega^{\frac{\mu+1}{2}}} \exp\left(-\frac{\mu(\kappa+1)r^2}{\omega}\right)$$
$$\times I_{\mu-1}\left(2\mu\sqrt{\kappa(\kappa+1)}\frac{r}{\sqrt{\omega}}\right) \qquad (2)$$

which denotes the PDF of the $\kappa-\mu$ fading model [21]. In (2), $I_v(\cdot)$ represents the modified Bessel function of the first kind and order v, κ is the ratio of the total power of the dominant components (δ^2) to the total power of the scattered waves ($2\mu\sigma^2$), whereas $\mu > 0$ is related to the multipath clustering and σ^2 is the power of the scattered waves in each of the clusters. The corresponding mean signal power is given by $E[R^2] = \Omega = \delta^2 + 2\mu\sigma^2$, with $E[\cdot]$ denoting the statistical expectation. Based on this and by letting Ω vary according to the gamma distribution, the corresponding PDF is given by

$$f_\Omega(\omega) = \frac{\omega^{\alpha-1}}{\Gamma(\alpha)\beta^\alpha} \exp\left(-\frac{\omega}{\beta}\right), \quad \omega \geq 0 \qquad (3)$$

where $\alpha > 0$ and $\beta > 0$ denote the shape and scale parameters respectively and $\Gamma(\cdot)$ is the gamma function. By substituting (2) and (3) into (1), the PDF of the composite signal envelope in a $\kappa-\mu$/gamma composite fading channel can be expressed in (4) as shown at the bottom of the next page.

TABLE I
PARAMETERS OF THE $\kappa-\mu$/GAMMA COMPOSITE FADING MODEL FOR A NUMBER OF SPECIAL CASES

Special Cases	Parameters of the $\kappa - \mu$ / gamma composite fading model			
	κ	μ	α	β
Rayleigh (Ω)	$\kappa \to 0$	$\mu = 1$	$\alpha \to \infty$	$\beta = \Omega$
Rice (K, Ω)	$\kappa = K$	$\mu = 1$	$\alpha \to \infty$	$\beta = \Omega$
Nakagami-m (m, Ω)	$\kappa \to 0$	$\mu = m$	$\alpha \to \infty$	$\beta = \Omega$
$\kappa - \mu$ (κ, μ, Ω)	$\kappa = \kappa$	$\mu = \mu$	$\alpha \to \infty$	$\beta = \Omega$
Rayleigh / gamma (α, β)	$\kappa \to 0$	$\mu = 1$	$\alpha = \alpha$	$\beta = \beta$
Nakagami / gamma (m, α, β)	$\kappa \to 0$	$\mu = m$	$\alpha = \alpha$	$\beta = \beta$
Rice / lognormal (K, u, σ)	$\kappa = K$	$\mu = 1$	$\alpha = \left[\exp\left(\sigma^2\right) - 1 \right]^{-1}$	$\beta = \exp\left(u + \frac{\sigma^2}{2}\right)\left[\exp\left(\sigma^2\right) - 1\right]$

Fig. 1.   PDFs of the $\kappa-\mu$/gamma composite fading model (continuous lines) for the special cases: $\kappa-\mu$ (circles), Nakagami-m (squares), Rice (triangles) and Rayleigh (asterisks) PDFs. The values of α and β of the $\kappa-\mu$/gamma composite fading model were 100 and 1.6, respectively.

Fig. 2.   PDFs of the $\kappa-\mu$/gamma composite fading model (continuous lines) which correspond to other composite fading models: Rayleigh/gamma [18] (circles); Rice/lognormal [17] (squares); and Nakagami/gamma fading [19] (triangles).

The $\kappa-\mu$/gamma composite fading model inherits all of the generality of the $\kappa-\mu$ distribution and therefore includes as special cases the one-sided Gaussian, Rice (Nakagami-n), Nakagami-m and Rayleigh distributions. For example, as shown in Fig. 1, as $\alpha \to \infty$ there is no shadowing of the mean signal power, and in this case, the $\kappa-\mu$/gamma composite fading model coincides with the $\kappa-\mu$ fading model [21]. Likewise, by setting $\mu = 1$ and again letting $\alpha \to \infty$, the Rice PDF can be obtained, where κ becomes equivalent to the Rice K factor [21]. Then, the Rayleigh distribution can be readily deduced by setting $\kappa = K = 0$. Similarly, the Nakagami-m distribution can be obtained by letting $\kappa \to 0$ with the μ parameter becoming equivalent to the m parameter of the Nakagami-m distribution [21]. Moreover, as shown in Fig. 2, the PDF of the $\kappa-\mu$/gamma composite fading model also includes as special cases other shadowed fading models such as the Rayleigh/gamma [18] and Nakagami-m/gamma [19] composite fading models. It is also worth noting that it can be used to provide an accurate approximation of the Rice/lognormal [17] composite fading model as shown
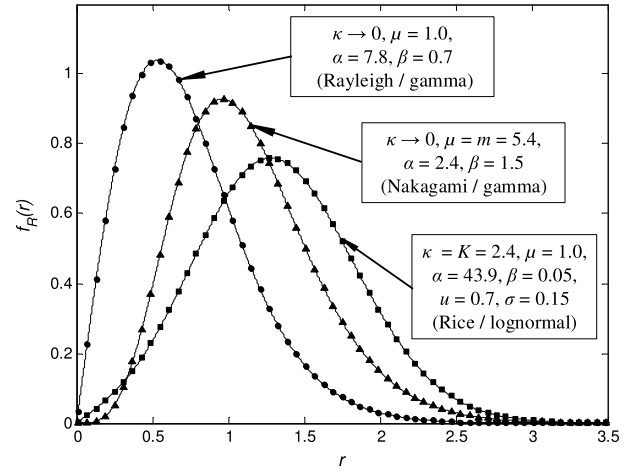
in Fig. 2. In this case, the log-scale parameter, u and shape parameter, σ of the lognormal distribution were estimated from parameters α and β of the gamma distribution with the aid of [22, eq. (6)]. Table I summarizes the parameters of the $\kappa-\mu$/gamma composite fading model for the special cases in which it coincides with the aforementioned fading models.

B. Probability Density Function

Having formulated the $\kappa-\mu$/gamma distribution in (4), we can derive a simple analytic expression for its envelope PDF. To this end, by expanding the $I_n(x)$ function in terms of the series representation in [23, eq. (8.445)], it immediately follows that

$$f_R(r) = \frac{2\mu(1+\kappa)^{\frac{\mu+1}{2}}r^\mu}{\kappa^{\frac{\mu-1}{2}}\exp(\mu\kappa)\beta^\alpha} \sum_{j=0}^{\infty} \frac{\left(\mu\sqrt{\kappa(\kappa+1)}r\right)^{\mu+2j-1}}{j!\Gamma(\alpha)\Gamma(\mu+j)}$$
$$\times \int_0^\infty \omega^{\alpha-\mu-j-1}\exp\left(-\mu(1+\kappa)\frac{r^2}{\omega}-\frac{\omega}{\beta}\right)d\omega \quad (5)$$

$$f_R(r) = \frac{2\mu(\kappa+1)^{\frac{\mu+1}{2}}r^\mu}{\kappa^{\frac{\mu-1}{2}}\exp(\mu\kappa)\Gamma(\alpha)\beta^\alpha}\int_0^\infty \omega^{\frac{2\alpha-\mu-3}{2}}\exp\left(-\mu(\kappa+1)\frac{r^2}{\omega}\right)\exp\left(-\frac{\omega}{\beta}\right)I_{\mu-1}\left(2\mu\sqrt{\kappa(\kappa+1)}\frac{r}{\sqrt{\omega}}\right)d\omega \quad (4)$$

$$F_R(r) = \sum_{j=0}^{\infty} \frac{\pi \kappa^j \mu^{\alpha+j}(1+\kappa)^{\alpha} x^{2\alpha} \, _1F_2\left(\alpha; \alpha - \mu - j + 1, 1 + \alpha; \frac{\mu(1+\kappa)x^2}{\beta}\right)}{j! \exp(\mu\kappa) \sin((\mu - \alpha + j)\pi) \beta^{\alpha} \Gamma(1 + \alpha - \mu - j)\Gamma(\mu + j)\Gamma(1 + \alpha)}$$
$$- \sum_{j=0}^{\infty} \frac{\pi \kappa^j \mu^{\mu+2j}(1+\kappa)^{\mu+j} x^{2\mu+2j} \, _1F_2\left(\mu + j; 1 + \mu - \alpha + j, 1 + \mu + j; \frac{\mu(1+\kappa)x^2}{\beta}\right)}{j! \exp(\mu\kappa) \sin((\mu - \alpha + j)\pi) \beta^{\mu+j} \Gamma(1 - \alpha + \mu + j)\Gamma(\alpha)\Gamma(1 + \mu + j)} \tag{8}$$

Notably, the integral in (5) can be expressed in closed-form with the aid of [23, eq. (3.471.9)]; therefore, by performing the necessary change of variables and substituting into (5) and carrying out long but basic algebraic manipulations, one obtains

$$f_R(r) = \sum_{j=0}^{\infty} \frac{4\mu^{\frac{\alpha+\mu+3j}{2}} \kappa^j (1+\kappa)^{\frac{\alpha+\mu+j}{2}} r^{\alpha+\mu+j-1}}{j! \exp(\mu\kappa)\Gamma(\alpha)\Gamma(\mu+j)\beta^{\frac{\alpha+\mu+j}{2}}}$$
$$\times K_{\alpha-\mu-j}\left(2r\sqrt{\frac{\mu(1+\kappa)}{\beta}}\right) \tag{6}$$

where $K_n(\cdot)$ denotes the modified Bessel function of the second kind and order n [23].

C. Cumulative Distribution Function

The cumulative distribution function (CDF) of the $\kappa-\mu/$gamma distribution can be readily obtained using the analytic expression derived for the PDF in (6). Based on this, one obtains

$$F_R(r) = \sum_{j=0}^{\infty} \frac{4\mu^{\frac{\alpha+\mu+3j}{2}} \kappa^j (1+\kappa)^{\frac{\alpha+\mu+j}{2}}}{j! \exp(\mu\kappa)\Gamma(\alpha)\Gamma(\mu+j)\beta^{\frac{\alpha+\mu+j}{2}}}$$
$$\times \int_0^x r^{\alpha+\mu+j-1} K_{\alpha-\mu-j}\left(2r\sqrt{\frac{\mu(1+\kappa)}{\beta}}\right) dr \tag{7}$$

The integral above can be expressed in closed-form with the aid of [24, eq. (1.12.1.2)], yielding (8) as shown at the top of this page where, $_pF_q(\cdot)$ denotes the generalized hypergeometric function [23], [24].

D. Moment Generating Function

Having derived the PDF of the $\kappa-\mu/$gamma distribution we can also proceed with the derivation of the corresponding moment generating function (MGF). To this end, one straightforwardly obtains

$$M_R(s) = \sum_{j=0}^{\infty} \frac{4\mu^{\frac{\alpha+\mu+3j}{2}} \kappa^j (1+\kappa)^{\frac{\alpha+\mu+j}{2}}}{j! \exp(\mu\kappa)\Gamma(\alpha)\Gamma(\mu+j)\beta^{\frac{\alpha+\mu+j}{2}}}$$
$$\times \int_0^{\infty} r^{\alpha+\mu+j-1} \exp(-sr)$$
$$\times K_{\alpha-\mu-j}\left(2r\sqrt{\frac{\mu(1+\kappa)}{\beta}}\right) dr \tag{9}$$

where the integral above can be expressed in closed-form using [23, eqs. (6.621.3) and (9.131.2)]. Therefore, by making the

necessary variable transformation and substituting in (9), the following exact analytic expression is deduced

$$M_R(s)$$
$$= \sum_{j=0}^{\infty} \frac{2\kappa^j (1+\kappa)^{\alpha} \mu^{\alpha+j} \Gamma(2\alpha)\Gamma(\mu-\alpha+j)}{j!(-1)^{\alpha-\mu} \exp(\mu\kappa)\Gamma(\alpha)\Gamma(\mu+j) s^{2\alpha}\beta^{\alpha}}$$
$$\times \, _2F_1\left(\alpha, \alpha + \frac{1}{2}; \alpha - \mu - j + 1; \frac{4\mu(1+\kappa)}{\beta s^2}\right)$$
$$+ \sum_{j=0}^{\infty} \frac{2\kappa^j (1+\kappa)^{\mu+j} \mu^{\mu+2j} \Gamma(\alpha-\mu-j)\Gamma(2\mu+2j)}{j!(-1)^{\alpha-\mu} \exp(\mu\kappa)\Gamma(\alpha)\Gamma(\mu+j) s^{2\mu+2j}\beta^{\mu+j}}$$
$$\times \, _2F_1\left(\mu + j, \mu + j + \frac{1}{2}; \mu - \alpha + j + 1; \frac{4\mu(1+\kappa)}{\beta s^2}\right) \tag{10}$$

where $_2F_1(\cdot)$ denotes the Gauss hypergeometric function [23], [24].

E. Moments and Amount of Fading

The PDF derived in (6) can also be used to obtain a simple analytic expression for the corresponding n moments. As a result, it immediately follows that the nth moment of the $\kappa-\mu/$gamma distribution can be expressed as follows:

$$E(R^n) = \sum_{j=0}^{\infty} \frac{4\mu^{\frac{\alpha+\mu+3j}{2}} \kappa^j (1+\kappa)^{\frac{\alpha+\mu+j}{2}}}{j! \exp(\mu\kappa)\Gamma(\alpha)\Gamma(\mu+j)\beta^{\frac{\alpha+\mu+j}{2}}}$$
$$\times \int_0^{\infty} r^{\alpha+\mu+n+j-1} K_{\alpha-\mu-j}\left(2r\sqrt{\frac{\mu(1+\kappa)}{\beta}}\right) dr \tag{11}$$

The integral above can be expressed in terms of the Euler gamma function $\Gamma(\cdot)$ [23, eq. (6.561.16)]; therefore, by performing the necessary change of variables and substituting into (11) yields

$$E(R^n) = \sum_{j=0}^{\infty} \frac{\mu^{j-\frac{n}{2}} \kappa^j \beta^{\frac{n}{2}} \Gamma\left(\alpha + \frac{n}{2}\right)\Gamma\left(\mu + j + \frac{n}{2}\right)}{j! \exp(\mu\kappa)\Gamma(\alpha)\Gamma(\mu+j)(1+\kappa)^{\frac{n}{2}}} \tag{12}$$

It is recalled here that the Pochhammer symbol is given by $(x)_n = \Gamma(x+n)/\Gamma(x)$ and thus, $\Gamma(x+n) = (x)_n \Gamma(x)$, [23]. To this effect, and again after long but basic algebraic manipulations, equation (12) can be equivalently re-written as

$$E(R^n) = \frac{\exp(-\mu\kappa)}{\Gamma(\alpha)\Gamma(\mu)} \left(\frac{\beta}{\mu(1+\kappa)}\right)^{\frac{n}{2}} \Gamma\left(\mu + \frac{n}{2}\right)$$
$$\times \Gamma\left(\alpha + \frac{n}{2}\right) \sum_{j=0}^{\infty} \frac{\left(\mu + \frac{n}{2}\right)_j}{(\mu)_j} \frac{(\mu\kappa)^j}{j!} \tag{13}$$

Importantly, the series representation above can be expressed in a simple closed-form yielding

$$E(R^n) = \frac{\exp(-\mu\kappa)}{\Gamma(\alpha)\Gamma(\mu)} \left(\frac{\beta}{\mu(1+\kappa)}\right)^{\frac{n}{2}} \Gamma\left(\mu + \frac{n}{2}\right)$$
$$\times \Gamma\left(\alpha + \frac{n}{2}\right) {}_1F_1\left(\mu + \frac{n}{2}; \mu; \mu\kappa\right) \qquad (14)$$

where ${}_1F_1(\cdot)$ denotes the Kummer confluent hypergeometric function [23], [24].

It is also recalled that the amount of fading (AF) is a useful performance metric in wireless communications over fading channels and its definition is given by [25, eq. (1.27)], namely

$$\text{AF} = \frac{E(X^2)}{[E(X)]^2} - 1 \qquad (15)$$

Therefore, the AF for the case of $\kappa{-}\mu$/gamma distribution can be readily expressed in closed-form by determining the corresponding first and second moments with the aid of (14), which yields

$$\text{AF} = \frac{\mu!\alpha!\Gamma(\mu)\Gamma(\alpha)\exp(\mu\kappa) {}_1F_1(\mu+1; \mu; \mu\kappa)}{\left[\Gamma\left(\mu + \frac{1}{2}\right)\Gamma\left(\alpha + \frac{1}{2}\right) {}_1F_1\left(\mu + \frac{1}{2}; \mu; \mu\kappa\right)\right]^2} - 1 \quad (16)$$

To the best of the authors' knowledge, the expressions derived above have not previously been reported in the open technical literature. Furthermore, because of their generality, they can be employed in the derivation of numerous useful performance metrics in digital communications over $\kappa{-}\mu$/gamma fading channels and the numerous special cases contained within.

III. MEASUREMENT SET-UP, ENVIRONMENTS AND EXPERIMENTS

A. Measurement Set-Up

The transmitter section of the channel measurement system consisted of an ML5805,[1] single chip fully integrated Frequency Shift Keyed (FSK) transceiver, manufactured by RFMD. It was configured to transmit a continuous wave signal with a power level of +17.6 dBm at 5.8 GHz. The transmit antenna was mounted tangentially with respect to the body surface of an adult male of height 1.83 m and mass 73 kg using a small strip of Velcro®. During the measurements, the transmitter was alternated between three different body locations on the test subject, as shown in Fig. 3(a). These were: the central-chest region at a height of 1.42 m; the central-waist region at a height of 1.15 m; and the right wrist region at a height of 0.98 m. Each of these hypothetical body worn node locations is likely to be used in future off-body systems. For example, the chest region is a suitable location for monitoring electrocardiogram (ECG), the waist region is a possible mounting point for a gateway node in a body area network (BAN), whereas the wrist region is a possible location for a smart watch.

It should be noted that in order to provide as realistic a characterization of the off-body channels as possible, the transmitter was attached, using the Velcro®, to the test subject's clothing for the chest and waist regions whereas it
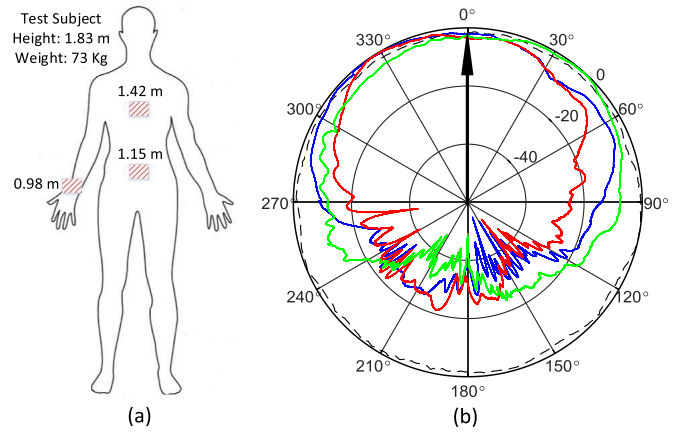

Fig. 3. (a) The three different hypothetical body worn node locations and (b) the measured azimuthal radiation patterns for the sleeve dipole antenna in free space (black dashed lines) and situated on the chest (red continuous lines), waist (blue continuous lines) and wrist (green continuous lines). It should be noted that the black arrow in (b) represents the direction that the test subject was facing.

was positioned next to his skin for the wrist region. The separation distances between the transmitter and the body for the three different body worn node locations were 5.8 mm, 7.5 mm and 4.0 mm for the chest, waist and wrist regions, respectively. It is well known that an antenna operating in the vicinity of the human body can introduce the complex antenna-body interaction effects such as power absorption, near-field coupling and radiation pattern distortion [26]. Fig. 3(b) shows the measured azimuthal radiation patterns for the sleeve dipole antenna in free space and situated on each body worn node position. As expected, due to the presence of the human body, it was obvious that the radiation patterns for all body worn node locations, particularly in the posterior direction (between 90° and 270°), were significantly distorted when compared to the radiation pattern in free space. Moreover, it was also observed that the radiation pattern in the anterior facing direction for the chest region was slightly more directional than those for the waist and wrist regions.

The receiver section of the channel measurement system, consisted of an antenna which was mounted vertically on a non-conductive polyvinyl chloride (PVC) stand at an elevation of 1.10 m above the floor level so that the antenna was parallel to the body worn nodes while the user was stationary. The antenna was connected to port 1 of a Rohde & Schwarz ZVB-8 vector network analyzer[2] (VNA) using a low-loss coaxial cable. A pre-measurement calibration was performed to reduce the effects of known system based errors using a Rohde & Schwarz ZV-Z51[3] calibration unit. This also enabled the elimination of the effects of the power amplifier and cable loss.

The VNA was configured as a sampling receiver, recording the magnitude of the b_1 wave quantity incident on port 1 with a bandwidth of 10 kHz, which was centered at the
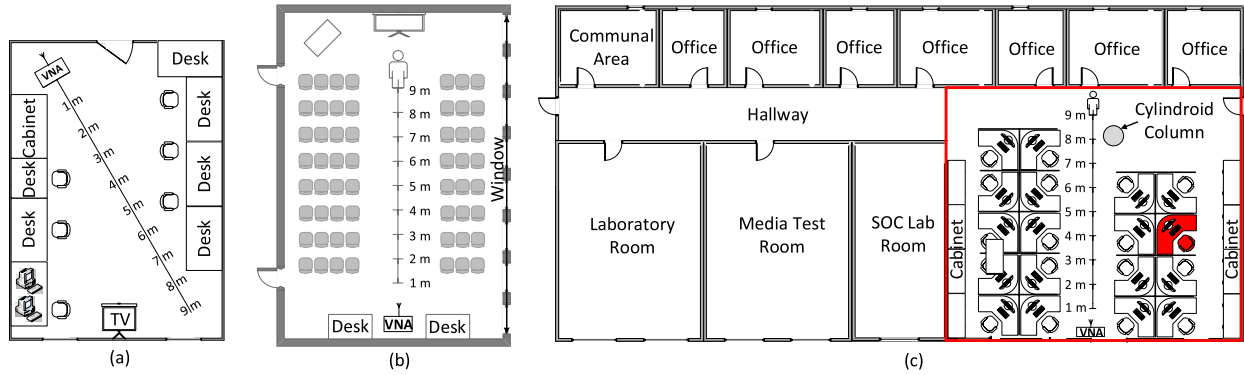
Fig. 4. Three different experimental environments: (a) Indoor laboratory (43.42 m^2), (b) Seminar room (99.63 m^2) and (c) Open office (red rectangle: 129.88 m^2). It should be noted that the desk filled with the red color in the open office area environment indicates that one person was working in this location during the measurements.

operation frequency. The magnitude of the b_1 measurements were automatically collected and stored on a laptop through a local area network (LAN) connection, providing an effective channel sampling frequency of 425.6 Hz (or equivalently a channel sample period of 2.3 ms). The average walking speed estimated from the channel data was 1.19 m/s, which equates to an average Doppler frequency [27] of 23.0 Hz. According to the Nyquist theorem, the required minimum sampling frequency must be at least twice the maximum Doppler frequency to avoid aliasing [28]; therefore, assuming that the human body was the main scattering object in the test environment, the given sampling frequency was more than adequate to characterize the time varying nature of the off-body communications channels studied here. The antennas used by both the transmitter and receiver were omnidirectional sleeve dipole antennas with +2.3 dBi gain (Mobile Mark model PSKN3-24/55S)[4] in free space.

B. Environments

To perform a robust characterization of the indoor off-body channel at 5.8 GHz, we conducted our experiments in a number of different indoor environments, in order to fully encapsulate variations in room size, materials and furniture. These locations were situated within the Institute of Electronics, Communications and Information Technology (ECIT) at Queen's University Belfast in the United Kingdom. They were: (1) an indoor laboratory environment with dimensions of 4.75 m × 9.14 m. The laboratory is situated on the 2nd floor of the ECIT building as shown in Fig. 4(a) and contained a number of chairs, boxes, lab equipment, metal cabinets and also desks constructed from medium density fiberboard. The laboratory was unoccupied for the duration of the experiments facilitating pedestrian free off-body channel measurements; (2) a seminar room with dimensions of 7.92 m × 12.58 m which is located on the 1st floor of the ECIT building as shown in Fig. 4(b). The seminar room contained a large number of chairs, desks, a projector and a white board. It also featured an external facing boundary wall constructed entirely from

glass with some metallic supporting pillars. Again, the seminar room was unoccupied for the duration of the experiments; (3) an open office area with dimensions of 10.62 m × 12.23 m situated on the 1st floor of the ECIT building as illustrated using the red rectangular outline in Fig. 4(c). The open office area contained a number of soft partitions, cabinets, PCs, chairs and desks. During the channel measurements, one person was working at his desk, as indicated with the red fill in Fig. 4(c). It is worth noting that all three environments also consisted of metal studded dry walls with a metal tiled floor covered with polypropylene-fiber, rubber backed carpet tiles, and metal ceiling with mineral fiber tiles and recessed louvered luminaries suspended 2.70 m above floor level.

C. Experiments

Four individual movement scenarios deemed likely to be encountered in everyday life were considered. These were: (1) walking in LOS conditions and (2) walking in non-LOS (NLOS) conditions, where the test subject walked towards and then away from the receiver in a straight line (from the 9 m point to 1 m point and vice versa as indicated in Fig. 4); (3) rotational movement, where the test subject rotated 360° in a clockwise direction from direct LOS through to the maximum shadowing condition (180° rotation) before returning to direct LOS at separation distances of 1 m, 5 m and 9 m from the receiver; (4) random movement, where the test subject walked randomly within a circle area with a radius of 1 m at separation distances of 1 m, 5 m and 9 m away from the receiver. It should be noted that unlike the classical indoor channel, the NLOS scenario considered in this study corresponds to the condition where the human body obscured the direct communication path between the body worn node and the receiver.

Due to the limitation of space, for the indoor laboratory environment, the random movement measurements were conducted at the separation distances of 1 m, 5 m and 8 m. The smallest data sets considered for the statistical analysis presented here were: 2401 for the LOS walking, 2251 for NLOS walking, 785 for the rotational movement and 4378 for the random movement. The mean recorded noise threshold in all three different indoor environments was observed to be

---

[4]http://www.mobilemark.com/wp-content/uploads/2015/04/antenna-spec-117-pskn3-2400.pdf (10/14/2015).
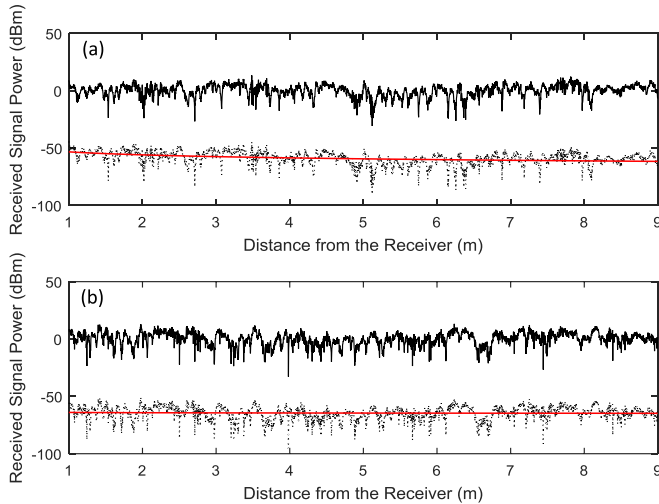
Fig. 5. Received signal power (black dotted lines) with a superimposed path loss fit (red continuous lines) alongside the abstracted composite fading component (black continuous lines) for the chest positioned antenna in the indoor laboratory environment for the (a) LOS and (b) NLOS walking scenarios during the 1st trial.

approximately -98.6 dBm. Moreover, the average walking speed and angular rotation speed were observed to be approximately 1.19 m/s and 2 rad/s, respectively. To improve the validity and robustness of the parameter estimates obtained in this study, measurements were repeated three times for all of the considered body worn node positions and movement scenarios within three different environments.

IV. RESULTS

The results presented in this section are expressed in terms of a simple path loss model and the composite fading signal. The log-distance path loss can be expressed as [27]

$$PL_{dB} = P(d_0)_{dB} + 10n \log \left(\frac{d}{d_0} \right) \qquad (17)$$

where P is the path loss at the reference distance d_0, n is the path loss exponent which indicates the rate at which the path loss increases with distance and d is the distance between transmit and receive antennas. The path loss at the reference distance and the path loss exponent were estimated using linear regression performed in MATLAB for both the LOS and NLOS walking scenarios. The reference distance, which should be in far field region of the antenna, was 1 m for all three environments considered in this study.

To abstract the composite fading signal for the LOS and NLOS scenarios, the elapsed time was first converted into a distance based upon an estimate of the test subject's velocity. The estimated path loss was then obtained using (17) and removed from the raw signal power. As an example, Fig. 5 shows the received signal power with a superimposed path loss fit alongside the abstracted composite fading components for the chest positioned antenna in the indoor laboratory environment while the test subject undertook the 1st trial of the LOS and NLOS walking scenarios. In the rotational and

random movement scenarios, as the test subject only moved over very small distances, the path loss was ignored and the global mean signal power was removed from the measured data. It is noted here that all parameters for the $\kappa-\mu$/gamma composite fading model were estimated using a non-linear least squares routine programmed in MATLAB. Furthermore, the integral in (4) was computed using `trapz` function which is also available in MATLAB.

A. LOS and NLOS Walking

The parameter estimates for n and P across all three environments are given in Table II along with the body shadowing factor (BSF) which is defined here as the difference between the path loss at the reference distance for the LOS and NLOS conditions. The parameter estimates presented here correspond to the mean values averaged over the three repeated trials in order to ensure their robustness. With the exception of the wrist position in the seminar room, for all of the hypothetical body worn node locations and environments, the path loss at the reference distance (P) for NLOS was greater than that for LOS due to the shadowing effects caused by the test subject's body. Also from Table II, it is clear that the values of the path loss exponent for the LOS walking movement scenario were smaller than that expected for free space ($n = 2$). This was likely due to the waveguide effect which can be present within indoor environments [29]. In fact, this phenomenon would have been particularly enhanced by the high metallic content of the walls and reinforced ceilings and floors. Similar results have been found for the off-body measurements conducted in [7] and [30]. The estimated path loss exponents for the NLOS walking scenario were relatively small compared to those obtained for the LOS case. This suggests that for short-range NLOS off-body channels, which suffer from bulk power absorption and body shadowing, the received signal is less dependent upon the distance between the body worn node and the receiver compared to the LOS case.

From Table II, it is evident that the lowest path loss at the reference distance and the highest path loss exponent over all of the three environments was observed for the LOS case with the transmitter on the waist. One possible explanation for this is that the height of the waist mounted transmitter (1.15 m) and the receiver (1.10 m) were almost the same, so the shortest propagation path between the transmitter and receiver was maintained while the test subject was walking. Also considering the values of the BSF given in Table II, it was observed that the wrist region had the least difference in path loss at the reference distance between the LOS and NLOS walking scenarios. This was due to the fact that as the test subject walked, his arms naturally moved between the front, side and back regions of the body. Therefore the wrist region can experience both the LOS and NLOS channel conditions irrespective of whether the person is walking towards or away from the receiver.

As an example of the results obtained from fitting the $\kappa-\mu$/gamma composite fading model to the off-body channel data, Table III depicts the mean parameter estimates for κ, μ, α and β during the LOS and NLOS walking scenarios in

TABLE II

AVERAGE ESTIMATED PATH LOSS PARAMETERS AND BODY SHADOWING FACTORS FOR EACH BODY WORN
NODE LOCATION AND ENVIRONMENT DURING THE LOS AND NLOS WALKING SCENARIOS

		LOS		NLOS		
		$\bar{n}$	$\bar{P}$ (dB)	$\bar{n}$	$\bar{P}$ (dB)	Av. BSF (dB)
Indoor Laboratory	Chest	1.04	51.3	0.17	63.5	12.2
	Waist	1.82	46.5	0.34	69.0	22.5
	Wrist	0.79	57.0	0.32	60.3	3.3
Seminar Room	Chest	0.91	56.1	0.71	64.5	8.4
	Waist	1.58	46.8	0.82	60.0	13.2
	Wrist	0.48	59.1	0.59	55.2	-3.9
Open Office Area	Chest	1.01	51.6	0.16	63.6	12.0
	Waist	1.79	46.4	0.26	69.5	23.1
	Wrist	0.72	57.3	0.36	60.0	2.7

TABLE III

AVERAGE PARAMETER ESTIMATES FOR THE $\kappa-\mu$/GAMMA COMPOSITE FADING MODEL DURING THE LOS AND
NLOS WALKING SCENARIOS FOR THE CHEST POSITION IN EACH ENVIRONMENT

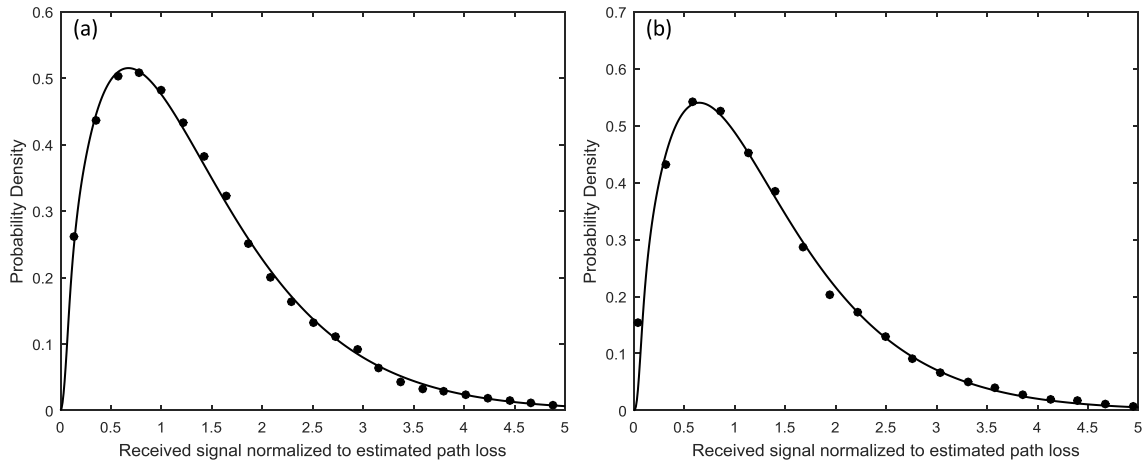|	LOS				NLOS			
	$\bar{\kappa}$	$\bar{\mu}$	$\bar{\alpha}$	$\bar{\beta}$	$\bar{\kappa}$	$\bar{\mu}$	$\bar{\alpha}$	$\bar{\beta}$
Laboratory	1.54	0.84	7.54	1.83	4.18	0.64	2.25	1.93
Seminar Room	3.36	0.58	1.15	2.30	5.56	0.47	1.02	2.45
Open Office	1.94	0.79	5.59	1.83	4.00	0.65	2.33	1.92

Fig. 6. Empirical PDFs (symbols) and $\kappa-\mu$/gamma composite fading PDFs (continuous lines) for the chest positioned antenna in the seminar room environment for the (a) LOS and (b) NLOS walking scenarios during the 3rd trial.

each of environments when the transmitter was positioned on the central-chest region. It became apparent that a resultant dominant signal component was always found to exist even for the NLOS walking scenario where the direct signal path was obscured by the test subject's body ($\kappa > 1$). This was most likely due to the fact that there existed dominant signal paths created by strong specular reflections in the surroundings and diffraction around the human body. Interestingly, the κ parameter for the NLOS case was greater

than that for the LOS case for all three environments, suggesting that in the NLOS channel the difference between the total power contributed by the dominant components and scattered contributions increased. One possible reason for this was that due to the shadowing effect of the human body, the power of the scattered components for the NLOS case were most likely to have been significantly weakened compared to the LOS case. Conversely, as the scattered contributions arriving from the field of view in the LOS scenario are less impacted

TABLE IV

AVERAGE PARAMETER ESTIMATES FOR THE $\kappa-\mu$/GAMMA COMPOSITE FADING MODEL FOR THE ROTATIONAL AND RANDOM MOVEMENT SCENARIOS FOR ALL BODY WORN NODE LOCATIONS AND ENVIRONMENTS

		Indoor Laboratory				Seminar Room				Open Office Area			
		$\bar{\kappa}$	$\bar{\mu}$	$\bar{\alpha}$	$\bar{\beta}$	$\bar{\kappa}$	$\bar{\mu}$	$\bar{\alpha}$	$\bar{\beta}$	$\bar{\kappa}$	$\bar{\mu}$	$\bar{\alpha}$	$\bar{\beta}$
		Rotational Movement											
Chest	1 m	0.01	0.99	1.08	3.17	0.01	1.04	1.36	2.48	0.01	1.26	1.88	1.11
	5 m	2.79	0.69	2.53	0.72	0.01	0.79	1.55	1.85	2.32	0.84	3.61	1.16
	9 m	5.71	0.66	6.03	0.49	4.67	0.56	1.53	2.54	5.42	0.52	4.22	1.31
Waist	1 m	0.06	0.79	1.01	4.83	0.01	0.94	1.14	2.65	0.01	0.88	1.26	3.10
	5 m	5.61	0.69	2.15	0.97	3.50	0.62	1.20	2.48	2.97	0.83	4.09	1.52
	9 m	6.82	0.51	9.14	0.52	3.28	0.64	2.84	1.21	3.56	0.78	7.31	0.26
Wrist	1 m	0.01	0.90	0.90	3.66	0.03	0.66	1.54	2.94	0.01	1.04	1.05	2.58
	5 m	2.30	0.69	2.00	1.10	3.81	0.58	1.38	2.15	1.80	0.69	7.48	0.40
	9 m	2.86	0.68	8.79	0.22	5.85	0.60	2.20	0.99	1.49	0.78	9.86	0.19
		Random Movement											
Chest	1 m	0.01	0.99	1.28	2.18	0.01	0.97	0.82	4.31	0.01	0.98	1.30	2.12
	5 m	1.46	0.85	2.05	1.04	0.01	0.97	0.94	3.36	1.63	0.83	1.95	1.11
	9 m	4.13	0.71	2.34	1.15	3.34	0.79	1.09	2.91	4.36	0.71	1.69	1.32
Waist	1 m	0.01	0.92	0.79	5.00	0.01	0.94	0.79	4.61	0.01	0.63	1.06	4.26
	5 m	4.09	0.61	1.55	1.44	6.67	0.55	1.30	1.97	4.33	0.59	1.51	1.48
	9 m	7.22	0.50	1.68	1.53	3.48	0.66	1.78	1.79	7.22	0.50	1.68	1.54
Wrist	1 m	0.01	1.05	1.11	2.46	0.01	0.95	1.58	2.13	0.01	1.08	1.10	2.44
	5 m	5.56	0.52	1.47	1.54	1.53	0.74	1.75	1.45	4.80	0.60	1.94	1.40
	9 m	6.67	0.51	2.61	1.39	2.94	0.65	1.77	1.48	6.80	0.51	2.23	1.41

by body shadowing their contribution is likely to have a more noticeable effect on the received signal resulting in lower κ parameter estimates. Nonetheless, it is worth highlighting that the increase in the κ parameter values when transitioning from LOS to NLOS occurs in the context of greater bulk power absorption and body shadowing. This can be seen from the BSF values reported in Table II, where there was more than a 10 dB reduction of the signal power when moving from LOS to NLOS for most body worn node positions.

The average estimated values of the μ parameter for all environments and hypothetical body worn node locations were smaller than 1 which suggests that the signal fluctuation in these channels is less impacted by scattering and determined more by the interaction of other multipath components. As anticipated, the values of α in the LOS case were greater than those for NLOS, meaning that the LOS walking scenario suffered less from shadowing than the NLOS case. As shown in Table III for the seminar room environment, occasionally the estimated shadowing parameters (α) obtained for LOS were found to be quite low, suggesting that these radio links experienced some shadowing even if a direct signal path existed. This observation was most likely caused by the fact that contributing signal components other than those arriving via LOS propagation (i.e. multipath components including both the dominant and scattered signal contributions) were shadowed by the human body and surrounding obstacles. As an example of the results of the model fitting, Fig. 6 shows the PDFs of the $\kappa-\mu$/gamma composite fading model fitted to the empirical data obtained for the chest positioned transmitter
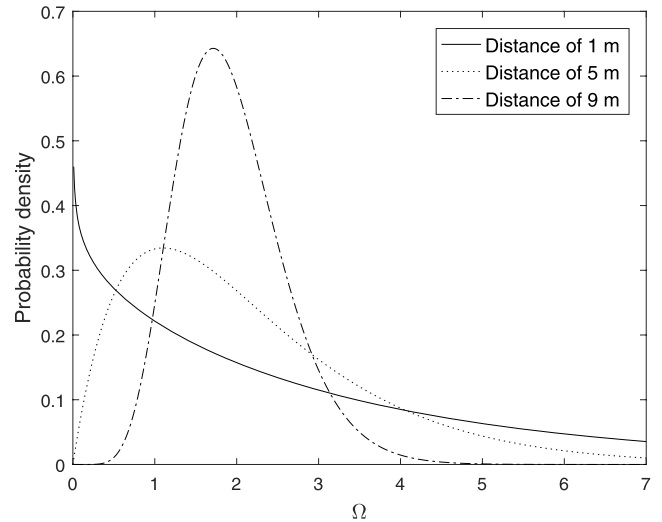

Fig. 7. PDFs of the mean signal power for the rotational movement at separation distances of 1 m, 5 m and 9 m for the wrist positioned antenna while the test subject was in the indoor laboratory environment. It should be noted that the mean values of parameter α and β in Table IV were used.

in the seminar room for both the LOS and NLOS walking scenarios during the 3rd trial. It is quite clear that the $\kappa-\mu$/gamma composite fading model provides an excellent fit to the empirical data for both of these scenarios.

B. Rotational and Random Movement

Table IV shows the mean value of the parameter estimates averaged over the three repeated trials for the rotational
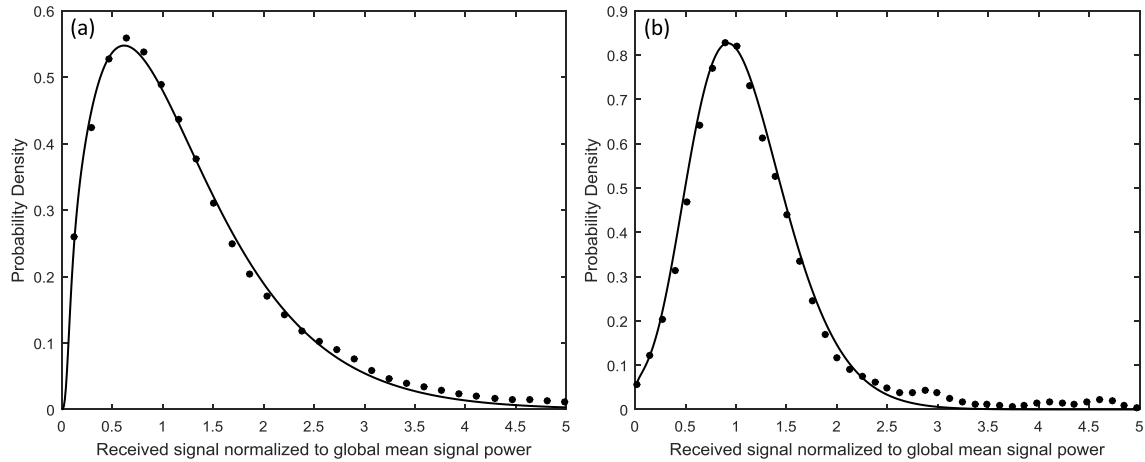
Fig. 8. Empirical (symbols) and $\kappa-\mu$/gamma composite fading PDFs (continuous lines) for the wrist positioned antenna during the 1st trial of the rotational movement at the 1 m location in (a) seminar room and (b) open office area environments.

and random movement scenarios. Again, a dominant signal component was found to exist for both scenarios. Here, the estimated κ parameters were greater than unity for nearly all cases with the exception of the measurements made at the 1 m point (and for the chest positioned device at the 5 m point in the seminar room). At these very short separation distances, the transmitted signal is extremely susceptible to shadowing effects caused by the human body. In this instance, due to the close proximity between the transmitter and the receiver it is unlikely that many dominant signal paths (e.g. strong specular reflections) are created that consistently carry significant power to the receiver. Instead, the signal reception will mostly be the result of shadowed diffuse contributions. This hypothesis is supported by the κ and μ parameters obtained for these scenarios. For all body worn node positions, over all three measurement environments and for the 1 m separation distance, the κ parameter was found to be close to zero and the μ parameter approached one. It is recalled here that when $\kappa = 0$ and $\mu = 1$, the $\kappa-\mu$/gamma composite fading model reduces to the Rayleigh/gamma composite fading model, which suggests that no dominant signal component was present and one cluster of shadowed multipath existed.

Fig. 7 illustrates the shadowing characteristics of the mean signal power for the wrist positioned transmitter during the rotational movement while the test subject was in the indoor laboratory environment. As we can see, when the distance between the hypothetical body worn node and the receiver was increased, the average estimated α value also increased (Table IV), meaning that there was less shadowing of the mean signal power. This observation may be explained using an extension of the rationale given above, that is, as the separation distance between the transmitter and the receiver was increased, more dominant signal paths were established which actively contributed to the received signal. These new dominant signal components act to increasingly stabilize the received signal and thus reduce the variation due to the shadowing effects. This trend was also observed for the rotational movement over all body worn node locations in the open office area environment.

In contrast, the average α parameters for the rotational measurements in the seminar room were less impacted by increases in the separation distance with only a very modest growth in these values (Table IV). This was most likely due to the spatial characteristics of this environment and the non-homogeneous physical make up of the room which featured an external facing boundary wall constructed entirely from glass with some metallic supporting pillars as well as the plasterboard bounding structures which featured prominently in the laboratory and open office environments. Therefore, as the person rotated, and largely irrespective of the distance, the receiver would have experienced different intensities of (shadowed) multipath depending on what bounding feature the test subject was facing towards. This effect was also prominent for the random movements in all three environments. Here, as the test subject moved around, he created a time-varying spatially distributed electromagnetic field pattern which in turn, was prone to shadowing depending upon the link geometry between the transmitter and receiver. This meant that the α parameters obtained were generally lower than those obtained for the other scenarios and also less sensitive to changes in the absolute straight line separation distance between the transmitter and receiver. As an example of the results of the model fitting for these scenarios, Figs 8 and 9 show the excellent agreement between the PDFs of the $\kappa-\mu$/gamma composite fading model and the empirical data obtained for the wrist positioned transmitter in the seminar room and open office area environments when the test subject performed a rotational movement at 1 m (Fig. 8) and random movement at 9 m (Fig. 9).

V. A COMPARISON WITH THE $\kappa-\mu$/LOGNORMAL LOS SHADOWED FADING MODEL

The $\kappa-\mu$/lognormal LOS shadowed fading model was recently proposed in [11] and has been successfully used to model the fading observed in body centric communications channels. Unlike the $\kappa-\mu$/gamma composite fading model, in a $\kappa-\mu$/lognormal LOS shadowed fading channel it is the LOS signal which only undergoes shadowed fading, with the
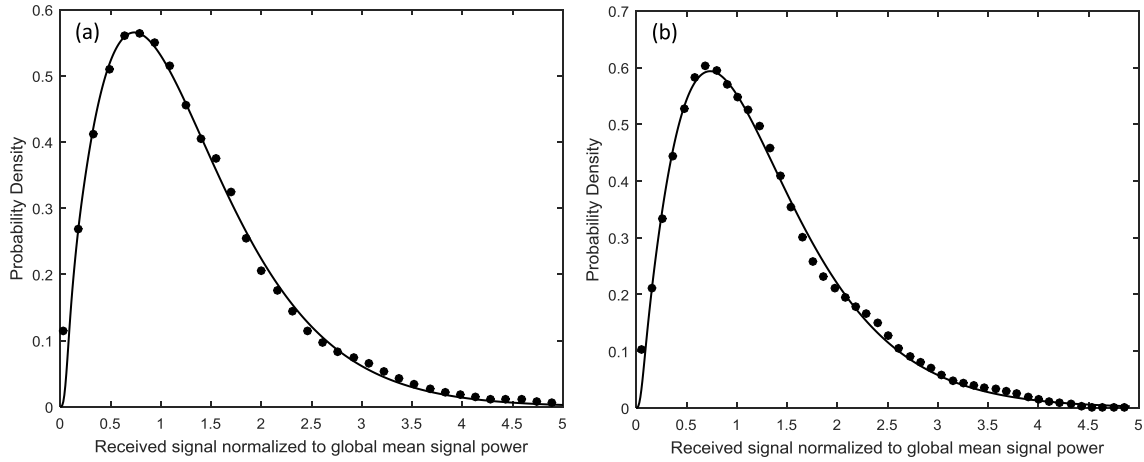
Fig. 9. Empirical (symbols) and $\kappa-\mu$/gamma composite fading PDFs (continuous lines) for the wrist positioned antenna during the 1st trial of the random movement at the 9 m location in (a) seminar room and (b) open office area environments.

TABLE V

AVERAGE VALUES OF THE KULLBACK-LEIBLER DIVERGENCE FOR THE $\kappa-\mu$/GAMMA COMPOSITE FADING MODEL AND THE $\kappa-\mu$/LOGNORMAL LOS SHADOWED FADING MODEL [11] FOR ALL OF THE CONSIDERED BODY WORN NODE POSITIONS AND MOVEMENT SCENARIOS WITHIN THREE DIFFERENT ENVIRONMENTS

		$\kappa-\mu$ / gamma			$\kappa-\mu$ / lognormal		
		Laboratory	Seminar	Open Office	Laboratory	Seminar	Open Office
LOS walking	chest	0.00496	**0.00332**	0.00409	**0.00408**	0.00422	**0.00299**
	waist	**0.00662**	**0.00166**	**0.00830**	0.01241	0.00468	0.01243
	wrist	**0.00338**	**0.00143**	**0.00477**	0.00690	0.00285	0.00497
NLOS walking	chest	**0.00316**	**0.00226**	**0.00201**	0.00611	0.00324	0.00415
	waist	**0.00459**	0.00272	**0.00381**	0.00679	**0.00261**	0.00390
	wrist	**0.00147**	**0.00163**	**0.00120**	0.00157	0.00275	0.00122
Rotation - 1 m	chest	**0.02015**	0.03447	0.03185	0.02825	**0.00656**	**0.01424**
	waist	**0.01568**	0.16102	**0.02933**	0.02825	**0.00916**	0.03610
	wrist	**0.02450**	**0.01440**	0.04545	0.02855	0.02160	**0.01265**
Rotation - 5 m	chest	**0.00683**	0.01086	**0.01130**	0.01093	**0.00324**	0.03781
	waist	0.02617	**0.00932**	0.02985	**0.01214**	0.01411	**0.01327**
	wrist	0.01211	**0.00950**	**0.00382**	**0.00692**	0.01143	0.00649
Rotation - 9 m	chest	0.01827	**0.00492**	0.02937	**0.00593**	0.00800	**0.02127**
	waist	0.02463	0.02160	0.02725	**0.00787**	**0.01347**	**0.02703**
	wrist	**0.00347**	**0.00540**	0.01210	0.00403	0.01083	**0.01130**
Random - 1 m	chest	**0.01723**	0.05617	**0.00903**	0.02267	**0.03330**	0.01227
	waist	**0.01237**	**0.01845**	**0.02933**	0.01787	0.03190	0.03610
	wrist	**0.02097**	**0.01440**	0.05833	0.02240	0.02160	**0.02573**
Random - 5 m	chest	**0.00543**	0.05177	0.01207	0.00573	**0.02993**	**0.00603**
	waist	**0.00567**	**0.00560**	**0.00740**	0.00757	0.01013	0.00930
	wrist	**0.00377**	**0.00460**	**0.00420**	0.00633	0.00577	0.00635
Random - 9 m	chest	**0.00199**	0.06243	**0.00830**	0.00861	**0.01895**	0.00935
	waist	**0.00297**	**0.00277**	0.00757	0.00557	0.01180	**0.00720**
	wrist	**0.00340**	0.01303	**0.00493**	0.00773	**0.00973**	0.00867

scattered multipath contribution remaining unperturbed by the shadowing effect. While both the dominant and scattered signal components can be shadowed together (e.g. due to the shadowing caused by the human body itself) it could be argued that in many instances, the overall contribution from the scattered components which are shadowed is likely to be so weak that it will not have a significant influence on the resultant signal. Therefore, to better understand the modes of propagation and hence the underlying signal models for the off-body channels studied in this work, we utilized the Kullback-Leibler divergence (D_{K-L}) to determine the information loss between the empirical PDFs and the theoretical PDFs for the $\kappa-\mu$/gamma composite and $\kappa-\mu$/lognormal LOS shadowed fading models.
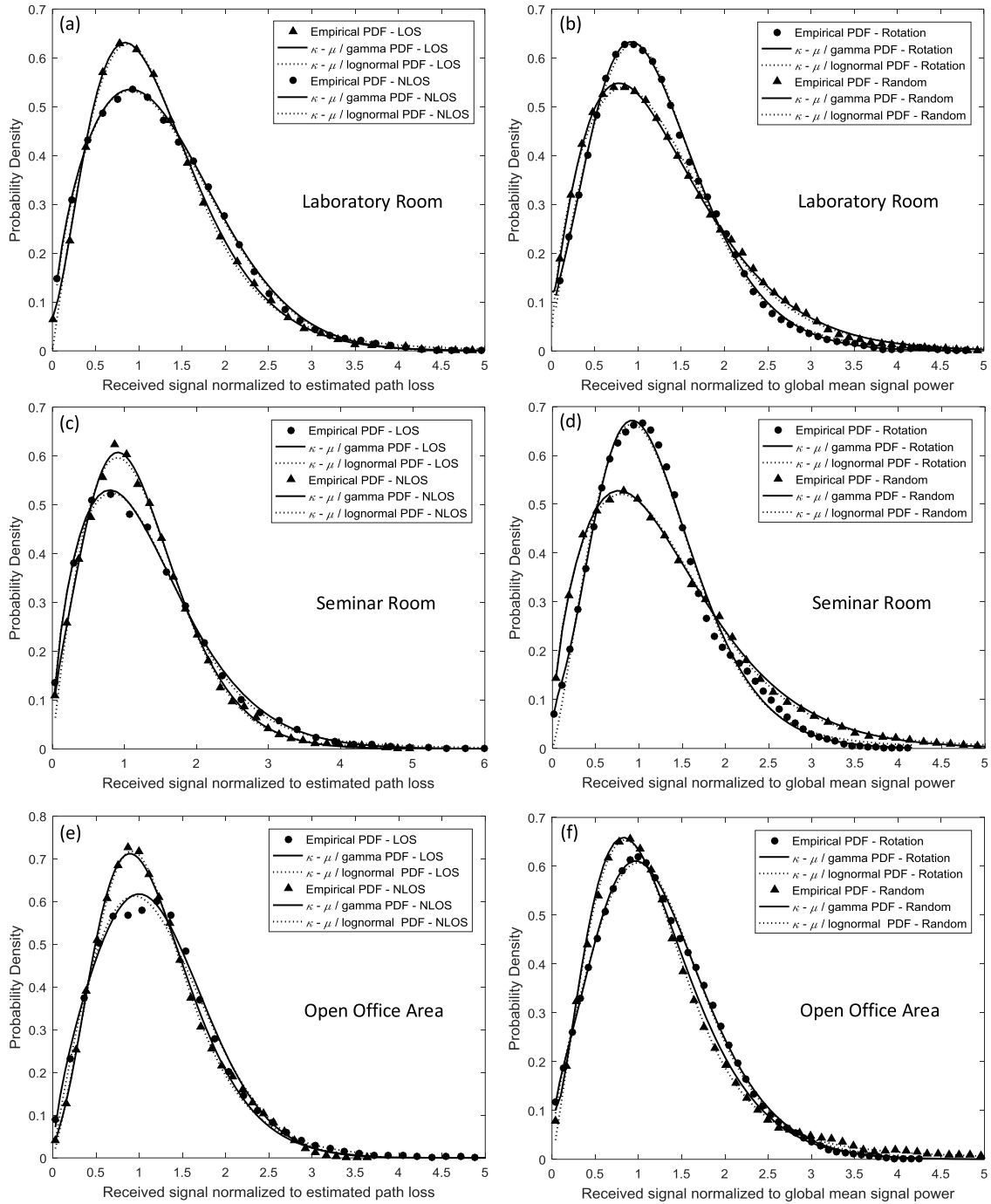
Fig. 10. Comparison of the two composite fading PDFs proposed in [11] and [20], along with the empirical PDFs for the LOS and NLOS scenarios during the 1st trial, the rotational movement scenario at 9 m during the 3rd trial and the random movement scenario at 1 m during the 1st trial for the wrist positioned antenna in all three indoor environments.

The Kullback-Leibler divergence, or relative entropy, quantifies the difference between two distributions and is defined as [31]

$$D_{K-L} = \int_{-\infty}^{\infty} f_1(x) \ln\left(\frac{f_1(x)}{f_2(x)}\right) dx \qquad (18)$$

where, in general, $f_1(x)$ represents the true PDF of the data and $f_2(x)$ denotes the test PDF, i.e. the approximated PDF of $f_1(x)$. Table V shows the mean values of the D_{K-L} averaged

over the three repeated trials for all of the considered body worn node locations and movement scenarios within three different environments. It was observed that the $\kappa-\mu$/gamma composite fading model provided a better fit compared to the $\kappa-\mu$/lognormal LOS shadowed fading model for approximately two-thirds of all of the considered data sets. This observation suggests that in the majority of cases considered here, measurable shadowing of both the dominant and scattered signal components was found to exist. Nonetheless, there

were still a significant number of scenarios for which the $\kappa-\mu$/lognormal LOS shadowed fading model outperformed the $\kappa-\mu$/gamma composite fading model (Table V). Thus, it can also be deduced that the impact of shadowing on the scattered signal contribution in some cases will be less apparent. Interestingly, as the separation distance between the transmitter and receiver was increased for both rotational and random movements, the number of cases for which the $\kappa-\mu$/ lognormal LOS shadowed fading model outperformed the $\kappa-\mu$/gamma composite fading model was slightly increased. This was most likely due to the fact that as the separation distance increased the total power of the scattered signal components became relatively so weak compared to that of the dominant signal components. As a consequence, in contrast with the LOS and NLOS cases, the resultant signal may not be significantly influenced by the shadowed scattered signal components.

As an example of the model fitting, Fig. 10 shows the empirical PDFs obtained for the wrist worn transmitter within all three indoor environments when the test subject performed the LOS, NLOS walking movements, a rotational movement at 9 m and random movement around the 1 m location. It can be seen that both composite fading models provided a good fit to the measured data although their D_{K-L} values appeared different.

VI. Conclusion

This paper investigated the shadowed fading in indoor off-body communications channels at 5.8 GHz. Novel analytic expressions were firstly derived for the PDF, CDF, moments and MGF of the $\kappa-\mu$/gamma composite model. Then, extensive measurements were carried out considering three different indoor environments and locations of a hypothetical body worn node along with four different types of user movement. From the estimated path loss exponents and path loss at the reference distance, it was found that the wrist region had less variations between the LOS and NLOS walking scenarios compared to the chest and waist regions. Additionally, it was found that for all of the indoor environments, irrespective of the hypothetical body worn node locations, path loss exponents for the LOS walking scenario were smaller than those generally anticipated for free space propagation, potentially due to the well-known waveguide effect often experienced within indoor environments. Over all of the measurement scenarios considered in this study, the PDF of the $\kappa-\mu$/gamma composite fading model has been shown to provide a good fit to the shadowed fading observed in indoor off-body communications channels. From the estimated parameters of this composite fading model, it was quite clear in many cases that the body shadowing and fading generated by the test subject's movement had a significant impact on indoor off-body communications channels. Using the Kullback-Leibler divergence, it has been shown that the $\kappa-\mu$/gamma composite fading model provided a better fit compared to the recently proposed $\kappa-\mu$/lognormal LOS shadowed fading model for approximately two-thirds of all the channels considered in this study.

As a final comment, when contrasting their complexity of implementation, both the native forms of the $\kappa-\mu$/gamma composite fading model and the $\kappa-\mu$/lognormal LOS shadowed fading model have four parameters, the modified Bessel function and require numerical integration. Therefore, in terms of complexity, their implementation is broadly similar and hence the choice between the two models will come down to the assumption of the propagation characteristics which seem most plausible. However, when it comes to analytical complexity, the $\kappa-\mu$/gamma composite fading model is more tractable as the derived analytic expressions for the PDF, CDF, moments and MGF can allow the derivation of explicit expressions for numerous performance measures of interests such as error probability and channel capacity, among others. On the contrary, this is currently not feasible for the $\kappa-\mu$/lognormal model due to the inherent algebraic complexity that typically renders relatively it intractable for further analysis.

References

[1] C. W. Kim, T. S. P. See, T. M. Chiam, Y. Ge, Z. N. Chen, and S. Sun, "Channel characterization of walking passerby's effects on 2.48-GHz wireless body area network," *IEEE Trans. Antennas Propag.*, vol. 61, no. 3, pp. 1495–1498, Mar. 2013.

[2] R. Rosini, R. Verdone, and R. D'Errico, "Body-to-body indoor channel modeling at 2.45 GHz," *IEEE Trans. Antennas Propag.*, vol. 62, no. 11, pp. 5807–5819, Nov. 2014.

[3] S. L. Cotton, A. McKernan, A. J. Ali, and W. G. Scanlon, "An experimental study on the impact of human body shadowing in off-body communications channels at 2.45 GHz," in *Proc. 5th Eur. Conf. Antennas Propag. (EuCAP)*, Apr. 2011, pp. 3133–3137.

[4] Q. H. Abbasi, M. M. Khan, S. Liaqat, A. Alomainy, and Y. Hao, "Ultra wideband off-body radio channel characterisation for different environments," in *Proc. 7th Int. Conf. Elect. Comput. Eng. (ICECE)*, Dec. 2012, pp. 165–168.

[5] M. Mackowiak and L. M. Correia, "Towards a radio channel model for off-body communications in a multipath environment," in *Proc. 18th Eur. Wireless Conf. (EW)*, Apr. 2012, pp. 1–7.

[6] S. L. Cotton and W. G. Scanlon, "Characterization and modeling of the indoor radio channel at 868 MHz for a mobile bodyworn wireless personal area network," *IEEE Antennas Wireless Propag. Lett.*, vol. 6, no. 11, pp. 51–55, Mar. 2007.

[7] R. Rosini and R. D'Errico, "Off-body channel modelling at 2.45 GHz for two different antennas," in *Proc. 6th Eur. Conf. Antennas Propag. (EuCAP)*, Mar. 2012, pp. 3378–3382.

[8] A. A. Goulianos, T. W. C. Brown, B. G. Evans, and S. Stavrou, "Wideband power modeling and time dispersion analysis for UWB indoor off-body communications," *IEEE Trans. Antennas Propag.*, vol. 57, no. 7, pp. 2162–2171, Jul. 2009.

[9] K. I. Ziri-Castro, W. G. Scanlon, and N. E. Evans, "Indoor radio channel characterization and modeling for a 5.2-GHz bodyworn receiver," *IEEE Antennas Wireless Propag. Lett.*, vol. 3, no. 1, pp. 219–222, Dec. 2004.

[10] C. Loo, "A statistical model for a land mobile satellite link," *IEEE Trans. Veh. Technol.*, vol. 34, no. 3, pp. 122–127, Aug. 1985.

[11] S. L. Cotton, "A statistical model for shadowed body-centric communications channels: Theory and validation," *IEEE Trans. Antennas Propag.*, vol. 62, no. 3, pp. 1416–1424, Mar. 2014.

[12] A. Abdi, W. C. Lau, M.-S. Alouini, and M. Kaveh, "A new simple model for land mobile satellite channels: First- and second-order statistics," *IEEE Trans. Wireless Commun.*, vol. 2, no. 3, pp. 519–528, May 2003.

[13] J. F. Paris, "Statistical characterization of $\kappa-\mu$ shadowed fading," *IEEE Trans. Veh. Technol.*, vol. 63, no. 2, pp. 518–526, Feb. 2014.

[14] S. L. Cotton, "Human body shadowing in cellular device-to-device communications: Channel modeling using the shadowed $\kappa-\mu$ fading model," *IEEE J. Sel. Areas Commun.*, vol. 33, no. 1, pp. 111–119, Jan. 2015.

[15] F. Hansen and F. I. Meno, "Mobile fading–Rayleigh and lognormal superimposed," *IEEE Trans. Veh. Technol.*, vol. VT-26, no. 4, pp. 332–335, Nov. 1977.

[16] H. Suzuki, "A statistical model for urban radio propogation," *IEEE Trans. Commun.*, vol. COM-25, no. 7, pp. 673–680, Jul. 1977.

[17] G. E. Corazza and F. Vatalaro, "A statistical model for land mobile satellite channels and its application to nongeostationary orbit systems," *IEEE Trans. Veh. Technol.*, vol. 43, no. 3, pp. 738–742, Aug. 1994.

[18] A. Abdi and M. Kaveh, "*K* distribution: An appropriate substitute for Rayleigh-lognormal distribution in fading-shadowing wireless channels," *IET Electron. Lett.*, vol. 34, no. 9, pp. 851–852, Apr. 1998.

[19] I. M. Kostić, "Analytical approach to performance analysis for channel subject to shadowing and fading," *IEE Proc.-Commun.*, vol. 152, no. 6, pp. 821–827, Dec. 2005.

[20] P. C. Sofotasios and S. Freear, "On the $\kappa-\mu$/gamma composite distribution: A generalized multipath/shadowing fading model," in *Proc. SBMO/IEEE MTT-S Int. Microw. Optoelectron. Conf. (IMOC)*, Oct./Nov. 2011, pp. 390–394.

[21] M. D. Yacoub, "The $\kappa-\mu$ distribution and the $\eta-\mu$ distribution," *IEEE Antennas Propag. Mag.*, vol. 49, no. 1, pp. 68–81, Feb. 2007.

[22] A. Abdi and M. Kaveh, "On the utility of gamma PDF in modeling shadow fading (slow fading)," in *Proc. IEEE 49th Veh. Technol. Conf. (VTC)*, vol. 3. Jul. 1999, pp. 2308–2312.

[23] I. S. Gradshteyn and I. M. Ryzhik, *Table of Integrals, Series, and Products*, A. Jeffrey and D. Zwillinger, Eds., 7th ed. London, U.K.: Academic, 2007.

[24] A. P. Prudnikov, Y. A. Brychkov, and O. I. Marichev, *Integrals Series: More Special Functions*, vol. 2, 3rd ed. New York, NY, USA: Gordon and Breach, 1992.

[25] M. K. Simon and M.-S. Alouini, *Digital Communication Over Fading Channels*, 2nd ed. New York, NY, USA: Wiley, 2005.

[26] P. Salonen, Y. Rahmat-Samii, and M. Kivikoski, "Wearable antennas in the vicinity of human body," in *Proc. IEEE Antennas Propag. Soc. Int. Symp.*, vol. 1. Jun. 2004, pp. 467–470.

[27] T. S. Rappaport, *Wireless Communications: Principles and Practice*. Upper Saddle River, NJ, USA: Prentice-Hall, 2002.

[28] F. P. Fontán and P. M. Espiñeira, *Modelling the Wireless Propagation Channel: A Simulation Approach With MATLAB*. New York, NY, USA: Wiley, 2008.

[29] A. A. M. Saleh and R. A. Valenzuela, "A statistical model for indoor multipath propagation," *IEEE J. Sel. Areas Commun.*, vol. SAC-5, no. 2, pp. 128–137, Feb. 1987.

[30] M. Mackowiak and L. M. Correia, "Statistical path loss model for dynamic off-body channels," in *Proc. IEEE 25th Annu. Int. Symp. Pers., Indoor, Mobile Radio Commun. (PIMRC)*, Sep. 2014, pp. 53–57.

[31] S. Kullback, *Information Theory and Statistics*. North Chelmsford, MA, USA: Courier Corporation, 1997.

Simon L. Cotton (S'04–M'07–SM'14) received the B.Eng. degree in electronics and software from the University of Ulster, Ulster, U.K., in 2004, and the Ph.D. degree in electrical and electronic engineering from Queen's University Belfast, Belfast, U.K., in 2007. He is currently a Reader in wireless communications with the Institute of Electronics, Communications and Information Technology, Queen's University Belfast. He is also a Co-Founder and the Chief Technology Officer of ActivWireless Ltd., Belfast. He has authored or coauthored over 90 publications in major IEEE/IET journals and refereed international conferences, two book chapters, and two patents. His research interests are cellular device-to-device, vehicular, and body-centric communications. His other research interests include radio channel characterization and modeling and the simulation of wireless channels. He received the H. A. Wheeler Prize, in 2010, from the IEEE Antennas and Propagation Society for the best applications journal paper in the IEEE TRANSACTIONS ON ANTENNAS AND PROPAGATION in 2009. In 2011, he also received the Sir George Macfarlane Award from the U.K. Royal Academy of Engineering in recognition of his technical and scientific attainment since graduating from his first degree in engineering.

Paschalis C. Sofotasios was born in Volos, Greece, in 1978. He received the M.Eng. degree from the University of Newcastle upon Tyne, U.K., in 2004, the M.Sc. degree from the University of Surrey, U.K., in 2006, and the Ph.D. degree from the University of Leeds, U.K., in 2011. His master's studies were funded by a scholarship from U.K.-EPSRC and his Ph.D. studies were sponsored by U.K.-EPSRC and Pace plc. He was a Post-Doctoral Researcher with the University of Leeds until 2013 and a Visiting Research Scholar with the University of California at Los Angeles, Los Angeles, CA, USA, in 2011. Since Fall 2013, he has been a Post-Doctoral Research Fellow with the Department of Electronics and Communications Engineering, Tampere University of Technology, Finland and the Wireless Communications Systems Group, Aristotle University of Thessalonki, Greece. His research interests are in the areas of fading channel characterization, cognitive radio, cooperative communications, and optical wireless communications, and in the theory and properties of special functions and statistics. He received an Exemplary Reviewer Award from the IEEE COMMUNICATION LETTERS in 2012 and from the IEEE TRANSACTIONS ON COMMUNICATIONS in 2015 and 2016, while he was a recipient of the Best Paper Award at ICUFN'13.

Seong Ki Yoo received the B.Eng. (Hons.) degree in telecommunication systems from the University of Surrey, Guildford, U.K., in 2010, and the M.Sc. degree in communications and signal processing from Imperial College London, London, U.K., in 2012. He is currently pursuing the Ph.D. degree with Queen's University Belfast, Belfast, U.K. His Ph.D. studies have been sponsored by U.K.-EPSRC. His research interests include channel characterization and modeling for off-body wireless communications, wearable communications, and diversity in body-centric communications.

Steven Freear (S'95–M'97–SM'11) received the Ph.D. degree in 1997. Subsequently, he was with the electronics industry for seven years as a Medical Ultrasonic System Designer. He was appointed as a Lecturer (Assistant Professor) and then a Senior Lecturer (Associate Professor) with the School of Electronic and Electrical Engineering, University of Leeds, in 2006 and 2008, respectively. In 2014, he was appointed as a Visiting Professor with Georgia Tech. He teaches digital signal processing, VLSI and embedded systems design, and hardware description languages at both undergraduate and postgraduate levels. His main research interest is concerned with advanced analog and digital signal processing. He has been an Associate Editor of the IEEE TRANSACTIONS ON ULTRASONICS, FERRORELECTRICS AND FREQUENCY CONTROL since 2009, and was appointed as the Editor-in-Chief in 2013.